Title
Cement Seawater Battery Energy Harvester for Marine Infrastructure Monitoring

Journal
IEEE Sensors Journal, 14(3)

ISSN
1530-437X

Authors
Ouellette, Scott A
Todd, Michael D

Publication Date
2014

DOI
10.1109/jsen.2013.2290492

Peer reviewed

Cement Seawater Battery Energy Harvester for Marine Infrastructure Monitoring

Scott A. Ouellette and Michael D. Todd

***Abstract*—This paper presents a novel corrosion-based energy harvester designed for long-term operational deployments in marine infrastructure monitoring. A statistical approach is utilized to characterize the output power, and the results are applied as the basis for designing a complimentary low-power sensor node. Further statistical analyses are performed on the sensor node operation to ensure robust operation over a range of design and environmental parameters. This paper concludes with a method for estimating the volumetric size of the active component in the energy harvester for long-term operation by analyzing the power consumption of the power electronics.**

***Index Terms*—Energy harvesting, low-power electronics design, corrosion**

I. Introduction

Corrosion damage to the U.S. industry had an estimated annual cost of $137.9 billion in 2002. The U.S. infrastructure comprised 16.4% ($22.6 billion) of the annual cost. Further analysis shows that, of the five categories of infrastructure studied, highway bridges account for 37% ($8.3 billion) of the estimated annual cost, while waterways and ports are roughly 1% ($300 million) [1].

At present, the U.S. infrastructures (highway bridges, waterways, and ports) are routinely inspected using mostly the visual inspection (VI) technique [2], [3]. The VI technique fails to provide sufficient information on incipient corrosion damage to reinforcing steel, and, as such, there have been developments towards embedded sensing of reinforcing steel rebar corrosion by proactively interrogating for regions of chloride concentration [4], [5]. Since corrosion is an electrochemical process, there are methods to exploit the potential difference relative to a reference cell (e.g. copper – copper sulfate) as a means of detection [6]. This method assumes the system impedance to have a fundamental frequency dependence that is revealed via Nyquist plot when excited with a chirp signal.

In most active sensing approaches to structural health monitoring, the conventional power supply is a battery (e.g. NiCd, NiMH, etc.). However, conventional batteries have a finite power capacity, and most embedded sensing applications render battery replacement in the deployed state prohibitively difficult [7]. There is a trade-off between power demands and damage localization when considering active and passive sensing of corrosion in infrastructure health monitoring. One solution to this problem is to utilize the failure mechanism (corrosion) as the source of power for deploying a sensing strategy.

Corrosion has, on multiple occasions, been shown to be a viable source of energy for powering of sensing and control systems [8]–[10]. Past research initiatives utilizing magnesium anodes oxidized in seawater, for a Galvanic series corrosion process, have shown to be suitable for powering deep-sea systems, such as oil wells [11], and geophysical observation devices [12] for long-term operations. Though operating deep beneath the water surface reduces the potential for bio-fouling, it also reduces the concentration of oxygen available for the reduction reaction – requiring the battery design to have an open structure to ensure the free access of fresh seawater. Multi-cell / serially connected designs are subject to leakage currents between electrodes, resulting in undesired inter-cell corrosion, housing corrosion, and eventually battery failure. Due to the power demands of the submerged devices (15-25 W) for operational periods spanning multiple years, a DC-DC converter, and, sometimes, a secondary battery are required for the single cell design. Other researchers have used the corrosion of reinforcing steel in concrete structures as the working electrode for powering custom corrosion sensors embedded in the concrete slab [13], [14], [15].

This paper proposes the use of cement to limit in a passive manner the amount of consumable oxygen for low depth, low-power generation applications in monitoring marine infrastructure subject to corrosive attack. The following sections will describe in detail the design and corrosion chemistry of the Galvanic series cement seawater battery, and a complimentary low-demand power conditioning circuitry for enabling a low-power sensor node. Two battery specimens were fabricated and placed in a seawater bath for a period of two weeks. For the duration of the experiment, the specimens were tested continuously to observe the evolution of the power output. An equivalent circuit model of the cement seawater battery is verified and used in the design of the power condition circuit. Monte Carlo SPICE simulations of the

Manuscript received April 26, 2013. This work was supported by a National Science Foundation Graduate Research Fellowship (NSF-GRFP).

S. A. Ouellette is with the Structural Engineering Department, University of California, San Diego, CA 92093 USA (e-mail: souellet@ucsd.edu).

M. D. Todd is with the Structural Engineering Department, University of California, San Diego, CA 92093 USA (e-mail: mdtodd@ucsd.edu).

power electronics are performed in order to verify a stable operation under variations in component tolerances and supplied power. The paper concludes with a calculation of the necessary anode volume for an operational deployment lifetime on the order of a host marine structure.

Specific contributions made in this paper to the field of energy harvesting include the novel use of cement as a passive corrosion rate limiter for prolonging the operational lifetime of a Galvanic-type corrosion battery of a fixed volume. Additionally, the Thévenin equivalent circuit model is experimentally validated, with the measured parameters used for the design of complimentary low-demand power electronics. Finally, uncertainty associated with the output power of the energy harvester is experimentally quantified and propagated to Monte Carlo simulations of the operation of the power electronics to provide a useful statistical performance assessment.

II. Cement Sea-water Battery

The concept for the cement battery was inspired by the need to monitor the health of reinforced concrete marine structures (e.g. bridges, piers, ports, etc.), in which one of the main damage modes of marine structures is due to the corrosion of steel.

Steel corrosion is the process in which iron atoms are removed from the surface by an electrochemical reaction, and subsequently dissolved into the surrounding electrolyte solution. In the case of reinforcing steel in concrete, the corrosion process only occurs at instances where pores meet the steel surface. The electrochemical process requires the transfer of electrons from the anode site (where the steel is losing mass) to the cathode site. These reactions occur simultaneously and are referred to as a redox reaction. The steel at the anode is oxidized (loses electrons) by the solution, and another location on the surface is reduced (accepts electrons). The corrosion process itself is electrochemical, and therefore can be exploited for electrical energy, as there is a transfer of electrons (current) as well as an activation voltage (i.e., the electromotive force).

A. Chemical Process Model

The cement battery operates via Galvanic corrosion, in which two dissimilar metals are immersed in a common electrolyte and share electrical contact. In the case of the cement battery, the electrodes are connected by a resistive load. The total electrochemical potential of the energy harvester is the sum of the half-cell potentials of the anode and cathode [16]. A major advantage in using the Galvanic series corrosion scheme is the cathodic protection of the more noble metal, which is carbon in this case. This model could prove to be useful in the corrosion defense of reinforced concrete structures by creating a Galvanic series battery using magnesium and steel. By using magnesium as a sacrificial anode, it is possible to design an energy harvester that both protects a significant bearing structural element from corrosive attack, and still provides simultaneously, sufficient power for a wireless sensor.

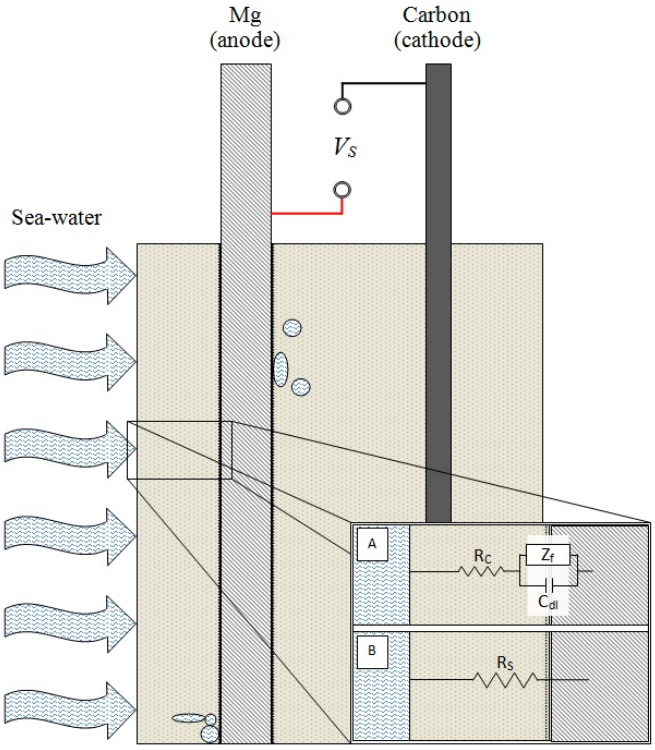

Fig. 1. A cross-section of the cement seawater battery design. The breakout image shows the conventional equivalent circuit for metallic corrosion in cement (A) and the model used in this study (B).

Due to their high relative electrical potential, the electrodes selected for the cement battery are magnesium (Mg) and carbon. Based on the Galvanic series for corroding metals, the expected output voltage for the energy harvester is ~ 1.8 V. The magnesium samples used in this study are from a generic water heater unit since it was easier to procure, in the correct shape (cylinder), and of affordable cost. The specific properties of the samples were not listed by the manufacturer, and, based on the experimental results, we have concluded that the sample was not pure magnesium. However, for the purposes of this paper, the equivalent circuit model and power conditioning circuitry are intended to be robust to variation.

Under uniform corrosive attack in an aqueous solution, the chemical process can be described by

$$\begin{aligned} Mg &\rightarrow Mg^{2+} + 2e^- \\ O_2 + 2H_2O + 4e^- &\rightarrow 4OH^-. \end{aligned} \quad (1)$$

Since there are no carbon ions in the electrolyte to be reduced to carbon atoms for a cathode reaction, oxygen and water molecules will react to form hydroxyl ions [16]. This reaction occurs because the pH of seawater ranges from basic to neutral depending on local environmental conditions [17]. Charge neutrality will impose on (1) that two magnesium atoms will be oxidized on the surface for each reduced oxide molecule.

There are some additional aspects of the chemical process of this battery unique to the design implementation of the cement cover. As a result of the porous structure of the cement, the magnesium anode will start to exhibit pitting corrosion at the local metallic surface sites where a cement

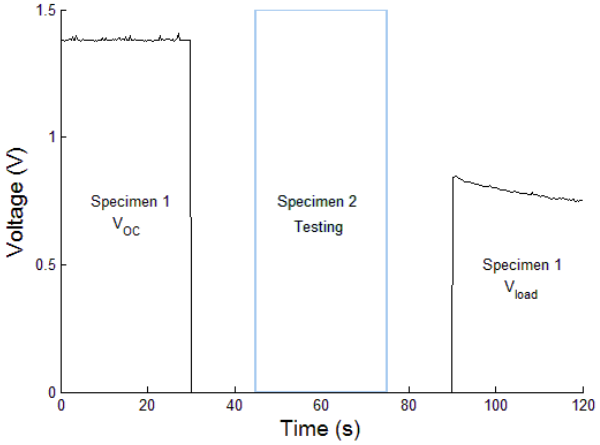

Fig. 2. Voltage trace as stored on the DAQ detailing the testing protocol.

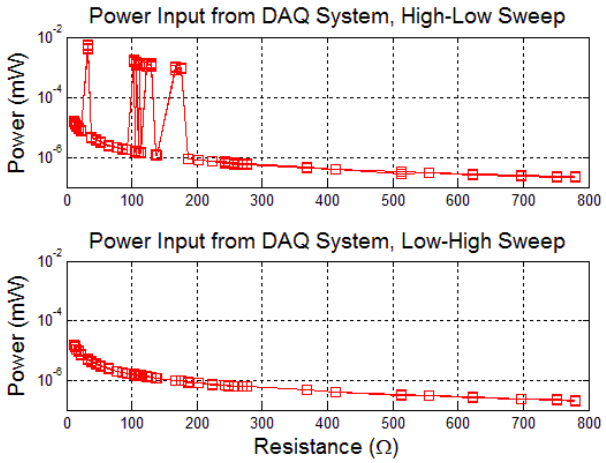

Fig. 3. Power contamination from DAQ on the high-to-low resistor board sweep tests.

pore is filled with seawater. This compositional heterogeneity results in a local increase in the corrosion rate of the anode. The oxidation reaction that takes place is the same as indicated in (1); however, the increased concentration of metal ions requires a proportional increase in chloride ions to sustain charge neutrality in the pit. A highly acidic by-product of the charge neutrality condition causes an additional increase in the corrosion rate, and the entire process would become autocatalytic if not for the limited rate of oxygen diffusion to the pitting site. The pitting reaction is shown below in (2).

$$Mg(Cl)_2 + 2H_2O \rightarrow Mg(OH)_2 + 2HCl \qquad (2)$$

The by-product of the corrosion process for the cement battery is insoluble magnesium oxide. Consequently, this battery design suffers from a similar issue with reinforced concrete in that the resulting deposits generate expansive stresses on the cement cover, which, if left unabated, can result in cracking.

B. Equivalent Circuit Model

For this work, Thévenin's equivalent circuit is used to model the cement seawater battery. As shown in Figure 1, the energy harvester is modeled as an ideal voltage supply with an

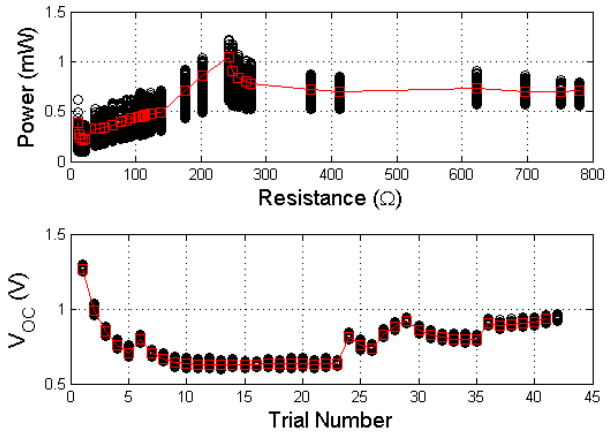

Fig. 4. Measured power output characteristics of cement battery with Thévenin model overlayed (top). The open-circuit voltage (bottom) for the resistor sweep test is used to iteratively calculate the expected power using (3).

ideal series resistor representing the resistivity of the cement barrier between the electrodes. More accurate models for corrosion of reinforcing metals in concrete with seawater as the electrolyte exist [18], [19]. These models feature an additional series capacitor and resistor in parallel to each other in order to approximate the surface resistance and capacitance to charge transfer. This paper is mainly focused on the dominant resistive behavior of the cement as it pertains to the total output power characteristics as a DC source, and therefore will ignore the second-order effects of frequency dependence in the corrosion process [20].

The application of Ohm's Law and the equation for electrical power can be used to determine the power (P_L) supplied to a resistive load (R_L):

$$P_L = V_S^2 \frac{R_L}{(R_S + R_L)^2}, \qquad (3)$$

where, V_S, and R_S are the equivalent source voltage and resistance for the cement battery, respectively. The implications of (3) dictate that the maximum power extracted from the battery occurs when $R_S = R_L$, the condition for impedance matching.

C. Test Setup and Results

The galvanic series cement batteries were tested over the course of 9 days in a controlled seawater bath at the Scripps Institution of Oceanography (SIO). The testing procedure was designed as a resistor sweep over 50 discrete resistance values in which the voltage across the load resistance was measured. In between each load resistance measurement trial, a baseline measurement of the open-circuit voltage of the cement battery specimen was obtained. Each trial, in which the cement battery specimen was connected to a load resistance, lasted 30 s. The NI PXI 1042Q (National Instruments) data acquisition (DAQ) controller would then switch the NI TB-2627 multiplexer (MUX) to connect the other specimen to perform the same test. As shown in Fig. 2, there was a programmed 15

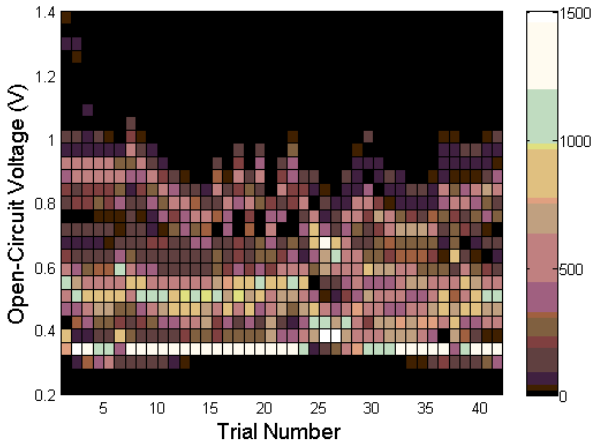

Fig. 5. Open-circuit voltage statistics for specimen 1. Each trial consists of a baseline open-circuit voltage measurement between connecting to a resistive load.

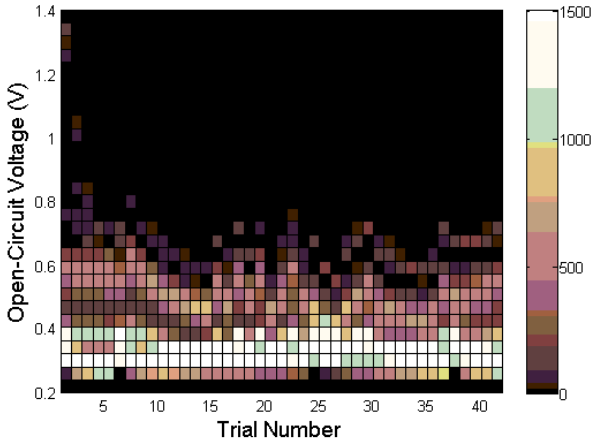

Fig. 6. Open-circuit voltage statistics for specimen 2.

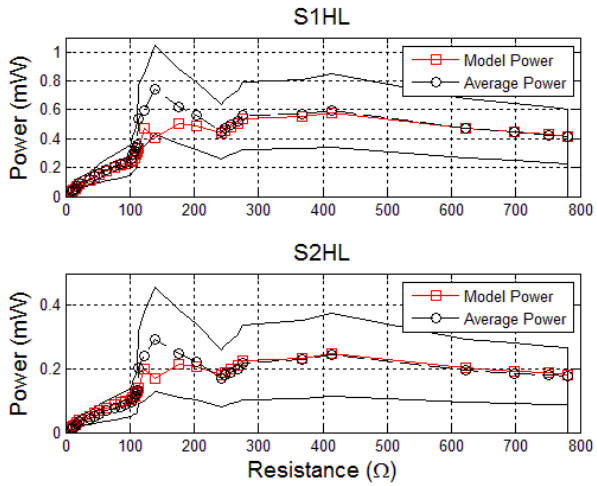

Fig. 7. Power output for high-to-low resistor sweeps for specimen 1 (top) and specimen 2 (bottom)

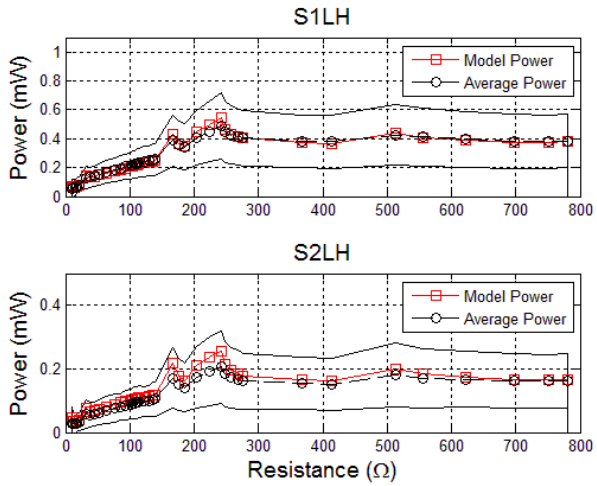

Fig. 8. Power output for low-to-high resistor sweeps for specimen 1 (top) and specimen 2 (bottom)

s delay in between each trial, and an open-circuit voltage measurement trial lasting 30 s was performed between each load resistance trial.

The resistor sweep was performed from low-to-high resistance for each specimen, and then from high-to-low resistance in the following test. This process occurred continuously for the duration of the experiment. The 50 discrete resistance values were placed on a custom designed and fabricated printed circuit board developed to interface with the MUX. The resistance values spanned the range from 10-800 Ω, with the highest value density in the range of 100-250 Ω in order to observe the peak power for each specimen and test. Each resistance value was connected to a specific channel on the MUX, and of the 50 values used, 9 suffered from connectivity issues. In addition, for tests in which the resistance values were swept from high-to-low values, an additional 8 channels suffered from cross-talk power corruption. The exact source of the cross-talk power is unknown; however, as seen in Fig. 3, this effect was quantified by running the DAQ tests with no external power connected to the resistor board.

When plotting the measured power versus the applied load resistance, the expected curve for a Thévenin circuit is not observed exactly. The reason for this is because the model assumes an ideal constant voltage source. The energy harvester, however, has a non-stationary voltage output as a result of several parameters involved in the corrosion process. Therefore, in order to correct for these variations, the open-circuit voltage measured prior to each resistive load trial is used as the representative source voltage for the model. The results show that the Thévenin model (shown in red) performs fairly well when compared to the data for each trial and test. For the results shown in Fig. 4, an assumed internal resistance of 200 ohms was used. Since the Thévenin model was accurate to within 4%, the internal resistance of the energy harvester can be determined by manipulating (3), the application of which yielded internal resistance values of ~ 200 and 250 ohms, respectively.

D. Statistical Properties of Battery Power

Due to the non-stationary characteristics of the corrosion process involved in generating the battery power, as well as

variations from specimen to specimen, a statistical approach to describing the energy harvester is used to assist with modeling the expected supply power to the sensor node. The parameters that can be varied for the energy harvesters design are as follows:

- Anode to cathode spacing
- Cathode to anode surface area ratio
- Cement cover thickness
- Water-cement ratio (a controlling parameter in cement porosity)
- Materials selection for anode and cathode (subject to Galvanic series)
- Oxygen concentration at cathode

Constraints with data acquisition hardware allowed for only two test specimens to be made with the varied parameter being cement porosity. The cement pastes were mixed with a water-cement ratio of 0.4 and 0.45, and air-cured for a period of 14 days. Under these conditions, the expected porosity is between 14.4-29.1% and 13.7-31.6% for w/c of 0.4 and 0.45, respectively [21]. The range of measured porosity percentage is an artifact of the method used.

The open circuit voltage statistics for each cement battery specimen are shown in Figs. 5 and 6. Each column in the above figures represents the sum of each histogram of the open circuit voltage measurements for a specific trial over the range of all tests. Thus, the first column represents all measured open circuit voltages at the start of each resistor sweep test.

The results indicate a large variation in the measured open-circuit voltage over the course of the experiment. Specimen 1 exhibits a near tri-modal voltage distribution, with the peaks at approximately 300 mV, 600 mV, and 900 mV. The statistics for specimen 2 have much less overall variation, but still exhibit the characteristic of multiple peaks.

For each specimen, the modal voltage is approximately 300mV, which is much lower than the designed output voltage of 1.6V. Furthermore, for both specimens, there appear to be outlier voltage measurements around 1.3V. The explanation behind this is actually rather simple in that these measurements indicate the first data points measured for the entire experiment. Factors contributing to the degradation of the output voltage of the battery grow in influence with time.

After processing the data, the cause of the output voltage disparity was determined to be rusted measurement probes. The rust was primarily confined to the carbon cathode/measurement interface as the probes were made of stainless steel. This event resulted in the DAQ measuring the voltage potential between the rust (most likely iron-oxide) and the magnesium hydroxide (an insoluble by-product of the corrosion process), which has significantly lower potential than the carbon/magnesium potential. Though measures were taken to avoid as much experimental error as possible, the longevity of the experiment combined with the test environment increased the occurrence of these experimental issues. This was an expected trade-off in reliability when deciding to automate the long-term measurement process.

The output power variability of each specimen is shown in Figs. 7 and 8. The figures show the measured mean power and one standard deviation, with the mean model power for comparison. The power characteristic for each sweep direction was analyzed separately as a metric of load response linearity. The results for both specimens show that there is a slight difference in the output power near matched impedance depending on the sweep direction. Though the Thévenin equivalent circuit model is linear, and thus does not exhibit a bias with regards to the load sweep direction, the results for each trial still validate the model with the only variation being the non-ideal source voltage, which is accounted for iteratively with a data-driven approach.

E. Cement Battery Capacity

When analyzing an energy harvester for its potential to be deployed in infrastructure monitoring scenarios, it is often instructive to compare the total available energy to that of more conventional power supply technology. A first-order corrosion rate model can estimate the current capacity of an anode of a given material by [16]

$$\frac{It}{V} = \frac{nF\rho}{M}, \tag{4}$$

where, I is anode current [mA], t is the time [hr], V is the anode volume accounting for porosity effects [cm^3], n is the number of electrons produced in the oxidation reaction, F is Faraday's constant [mA•hr mol^{-1}], ρ is the anode density [g cm^{-3}], and M is the anode atomic weight [g mol^{-1}]. The expression relates the current capacity per unit volume for a corroding metal anode encased in cement, where the porosity factor scales the amount of available surface area of the anode for corrosion initiation sites.

III. Power Conditioning Circuit

Using the cement seawater battery as an energy harvester only solves part of the overall monitoring problem. In order to acquire data on the health of a structure subject to corrosive attack, it is imperative that the energy produced by the batteries be used to power appropriate sensing electronics. However, based on the output voltage statistics of the cement seawater battery, the sensor node will require a DC-DC boost converter to accommodate the voltage requirements of a CMOS microcontroller. The DC-DC boost converter in this study is designed to convert low input voltages and output a feedback-regulated 3 V. The power supplied by the cement seawater battery is isolated from the boost converter and microcontroller by a low on-resistance analog switch in order to prevent continuous operation of the voltage conditioning circuitry. The analog switch is controlled by a low-power PWM timer IC.

A. Power Electronics Design

The power electronics employed in this sensor node design

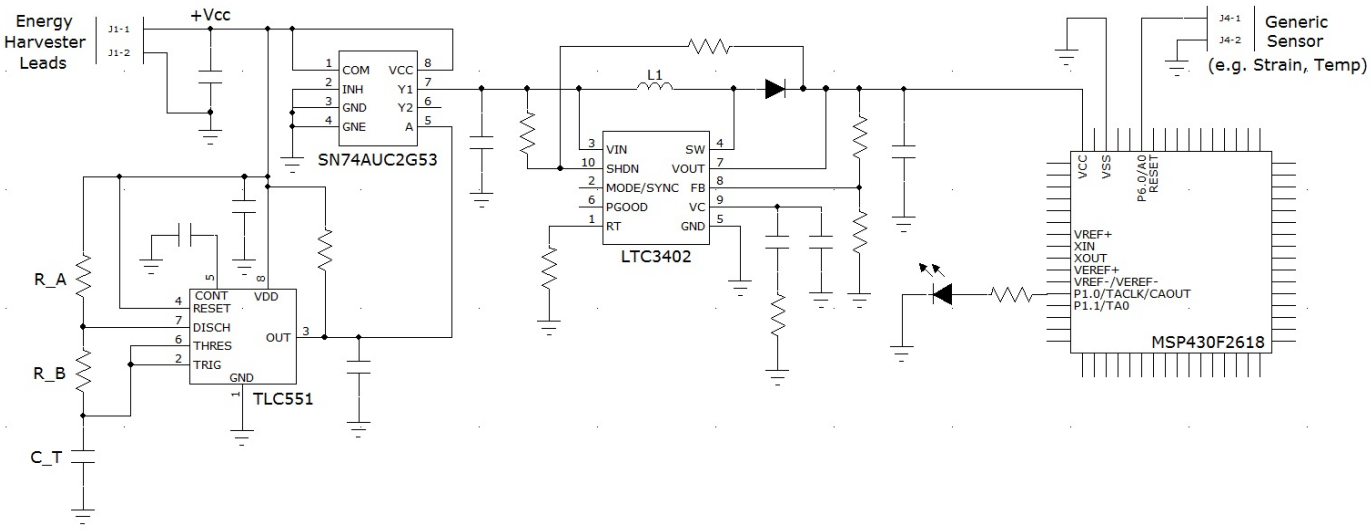

Fig. 9. Schematic of low-power sensor node.

features the use of a 100 mF storage capacitor as the main power supply. A schematic and photograph of the fabricated prototype sensor node are shown in Figs. 9 and 10, respectively. The capacitor is charged by the energy harvester and is isolated from the DC-DC boost converter by a low-voltage, low on-resistance SPDT analog switch (SN74AUC2G53, Texas Instruments), which is itself controlled by a low-voltage timer IC (TLC 551, Texas Instruments). The timer IC is set to generate a PWM voltage signal from GND to $+V_{cc}$ with a duty cycle that is higher than 99%. The approximate relation that defines the output PWM signal, neglecting propagation delay times within the internal architecture, is

$$t_{on} \approx C_t(R_A + R_B)ln2 \quad (5)$$

$$t_{off} \approx C_t R_B ln2, \quad (6)$$

where, C_t is the threshold capacitor, and R_A and R_B are the resistors through which it charges. Normally power savings result from operating at a duty cycle less than 50%; however, as suggested by (5) and (6), it is very difficult to operate the TLC 551 at duty cycles less than 50% due to the shared charge and discharge paths. Therefore, it is necessary to invert the PWM signal from high to low duty cycle. Instead of adding an inverter to the output of the timer IC, the output gate on the analog SPDT switch is chosen such that the supply capacitor drains when the control pin is low (GND). This effectively inverts the very high duty cycle output from the timer IC to a very low duty cycle gate signal on the SPDT analog switch. The component values are chosen such that the switch gate opens for 20ms, and closes for 60 s. The DC-DC boost converter is driven by a micro-power switching regulator (LTC3402, Linear Technology). The LTC3402 features a low startup voltage (0.85 V) and an adjustable output voltage from 2.6-5.5 V_{DC}. The discrete passive components (resistors, capacitors, and inductors) were selected such that the output voltage is set at 3 V. The microcontroller (MSP430f2618, Texas Instruments) requires a 515 µA supply current for a 3 V

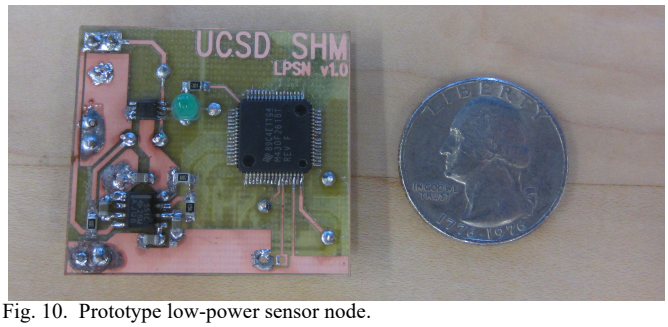

Fig. 10. Prototype low-power sensor node.

supply voltage when operating in active mode. Based on the documented performance of the LTC3402 operating in fixed-frequency mode (3MHz), the expected efficiency of the boost converter is approximately 50%, when supplying a light load of 515 µA. It is possible to push the efficiency to 70% if the switching regulator is set to BURST mode operation, which features an adaptive switching frequency.

B. SPICE Simulation and Monte Carlo Analysis

Circuit simulations were performed on an equivalent circuit model of the sensor node and power supply using LTSpice IV (Linear Technology). The supply power for the circuit comes from the 100 mF electrolytic capacitor set with an initial voltage range of 0.4-1.7 V. All of the discrete resistors and capacitors chosen were from the LTSpice IV ideal components library. The TLC551 timer IC was modeled as an ideal voltage source supplying a specified PWM signal, which is connected to the control pin on an idealized voltage-controlled switch used to model the SN74AUG2G53 analog switch. The PWM signal in this model is set to activate the analog switch gate at the intended duty cycle and duration described in the previous sub-section. The LTC3402 switching regulator is an empirically based sub-circuit component model that comes built-in with the software download.

The MSP430 was modeled as a piecewise linear varistor representing the power consumption when set in two different

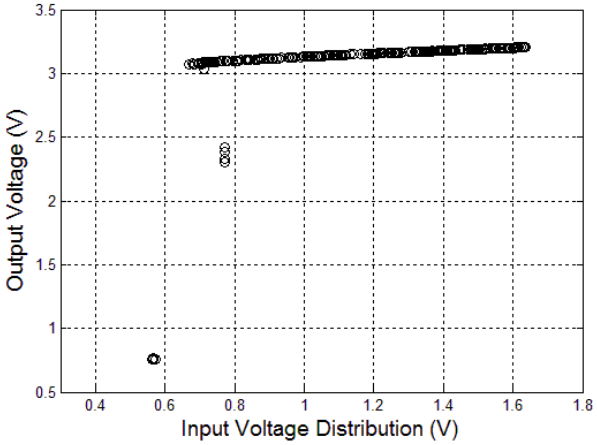

Fig. 11. Output voltage distribution of boost converter.

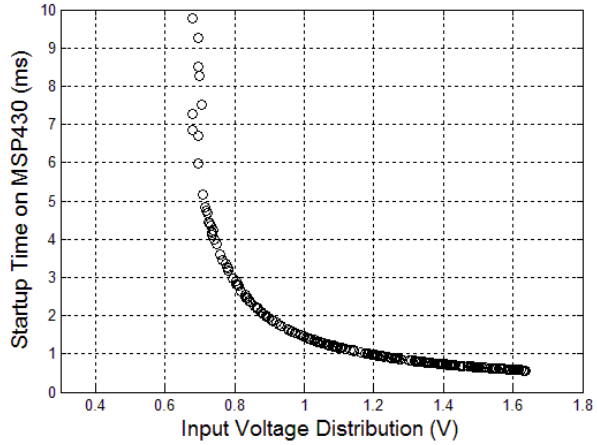

Fig. 12. Startup time on MCU as a function of input voltage variation.

operational modes, namely the active mode (AM), and low-power mode zero (LMP0). The effective resistance values for the two states were calculated from the known current consumption for a given supply voltage – either 2.2 V or 3 V [22].

Each discrete component has a manufacturer-defined tolerance, and in the case of the power inductor, the tolerance for the rated inductance is as high a 30%. A 250 run, 13-parameter Monte Carlo analysis was performed in order to observe the effect of component value and input voltage variability on the output power characteristics of the boost converter. Since the boost converter employs closed-loop regulated feedback architecture, there is little effect on the output voltage delivered to the microcontroller above input voltages of 800 mV, as seen in Figure 11. However, the variations do have an effect on the output rise time to the MSP430 startup voltage of 2.2 V. As seen in Figure 12, the rise time to the minimum microcontroller supply voltage of 2.2 V can vary from 1-10 ms. Furthermore, the startup time is asymptotic as the input voltage approaches 600 mV, which is expected as the rectifier diode requires 600 mV to conduct.

C. Power Consumption

The power consumption of the active electronic components will ultimately determine the operational lifetime of the cement seawater battery. By properly analyzing the current consumption of the power conditioning electronics and selected MCU, the necessary anode volume can be calculated for long-term (~50 years) operations in marine infrastructure monitoring.

Summing the power demands of the microcontroller, switching regulator, and timer IC results in an overall requirement of 3 mW. Since the LTC3402 switching regulator operates with a 50% efficiency based on the supply current demand of the MSP430, the supply power must be at least 6mW to operate the microcontroller.

Assuming the supply voltage is 1.3 V, the input current demand of the sensor node will be approximately 4.63 mA. Based on the sensor node design, the supply power will come from the 100 mF storage capacitor. For a 100 mF capacitor discharging a constant current, the total discharge time is determined by

$$\Delta t = \frac{C}{-i_{cap}}(V - V_i) \tag{7}$$

where, Δt is the total discharge time (s), C is the capacitance (Farad), i_{cap} is the capacitor current flowing into the sensor node (A), V is the final supply capacitor voltage (V), and V_i is the initial charge voltage of the supply capacitor. Assuming the current demand is constant, the discharge time across the synthetic load will be 28s.

Based on the experimental results, the total charge time for the 100 mF capacitor for an equivalent source resistance of 200 Ω is determined by

$$t_{charge} = -RC\, ln\left(\frac{V_S - \varepsilon/100}{V_S}\right), \tag{8}$$

where, V_s is the energy harvester source voltage (V), R is the equivalent source resistance (Ω), and ε is the percent decrease to which the capacitor will charge. Thus, for the supply capacitor to charge to within 1% of the source voltage, the total charge time will be approximately 98s.

Therefore, solving equation (7) for the capacitor current determines the amount of source current required to charge the capacitor to 1.3 V Since the necessary charge current is known, as well as the sensor node duty cycle, the necessary anode volume for 50 years of operation can be determined using equation (4).

IV. Conclusions

A passive diffusion controlled corrosion-based energy harvester designed for long-term marine infrastructure monitoring was presented. An equivalent circuit model was implemented and combined with a statistical approach to characterize the output power of the energy harvester. These

results were implemented and used as the basis in the design of a complimentary low-power sensor node. A 13-parameter Monte Carlo analysis was performed on the operation of the sensor node to ensure robust operation under a distribution of supplied power resulting from several design and environmental parameters in addition to component tolerance variability.

At present, the project is working towards the implementation of a low-power wireless transmitter-receiver network using the CC2571 (Texas Instruments) 2.4 GHz network processor operating with the ANT protocol. These devices are designed to seamlessly interface with the MSP430 family of microcontrollers. The additional supply current demand will ultimately reduce the overall operational lifetime for an anode of fixed volume; however, it will also improve the efficiency of the step-up converter.

Future work on this initiative involves the development of a low-power voltage threshold gate switch to create an adaptive duty cycle on the power drain from the main storage capacitor in order to further lengthen the lifetime of an anode of fixed volume. Additionally, further parametric studies on the energy harvester design could drastically improve the power output of the device without sacrificing the long-term operational lifetime.

ACKNOWLEDGMENT

The authors thank Dr. Steve Burrow from the University of Bristol for guidance on low-power electronics design and switched-mode power supplies. The authors also thank Richard Do, Cory Youngdale, and Joao Cheong for their assistance with co-executing experiments at SIO.

REFERENCES

[1] G. H. Koch, M. P. H. Brongers, N. G. Thompson, Y. P. Virmani, and J. H. Payer, “Corrosion cost and preventive strategies in the United States,” Turner-Fairbank Highway Research Center, 2002.

[2] B. Phares, G. Washer, D. Rolander, B. Graybeal, and M. Moore, “Routine Highway Bridge Inspection Condition Documentation Accuracy and Reliability,” *Journal of Bridge Engineering*, vol. 9, no. 4, pp. 403–413, 2004.

[3] R. B. Polder and M. R. De Rooij, “Durability of marine concrete structures-field investigations and modelling,” *HERON-ENGLISH EDITION-*, vol. 50, no. 3, p. 133, 2005.

[4] P. L. Fuhr, D. R. Huston, A. P. McPadden, and R. F. Cauley, “Embedded chloride detectors for roadways and bridges,” pp. 229–237, Apr. 1996.

[5] P. L. Fuhr, D. R. Huston, and B. MacCraith, “Embedded fiber optic sensors for bridge deck chloride penetration measurement,” *Opt. Eng*, vol. 37, no. 4, pp. 1221–1228, Apr. 1998.

[6] P. A. GAYDECKP and F. M. BURDEKIN, “Nondestructive Testing of Reinforced and Pre-Stressed Concrete Structures,” *Nondestructive Testing and Evaluation*, vol. 14, no. 6, pp. 339–392, 1998.

[7] G. Park, T. Rosing, M. Todd, C. Farrar, and W. Hodgkiss, “Energy Harvesting for Structural Health Monitoring Sensor Networks,” *Journal of Infrastructure Systems*, vol. 14, no. 1, pp. 64–79, 2008.

[8] M. Walsh, “Single cell seawater batteries,” in *Power Sources Symposium, 1990., Proceedings of the 34th International*, 1990, pp. 110–111.

[9] O. Hasvold, “Seawater batteries for low power, long term applications,” in *Power Sources Symposium, 1990., Proceedings of the 34th International*, 1990, pp. 50 –52.

[10] J. S. Lauer, J. F. Jackovitz, and E. S. Buzzelli, “Seawater activated power source for long term missions,” in *Power Sources Symposium, 1990., Proceedings of the 34th International*, 1990, pp. 115 –117.

[11] Ø. Hasvold, H. Henriksen, E. Melv‡r, G. Citi, B. Ø. Johansen, T. Kjønigsen, and R. Galetti, “Sea-water battery for subsea control systems,” *Journal of Power Sources*, vol. 65, no. 1–2, pp. 253–261, Mar. 1997.

[12] M. Shinohara, E. Araki, M. Mochizuki, T. Kanazawa, and K. Suyehiro, “Practical application of a sea-water battery in deep-sea basin and its performance,” *Journal of Power Sources*, vol. 187, no. 1, pp. 253–260, 2009.

[13] G. Qiao, G. Sun, Y. Hong, Y. Qiu, and J. Ou, “Remote corrosion monitoring of the RC structures using the electrochemical wireless energy-harvesting sensors and networks,” *NDT and E International*, vol. 44, no. 7, pp. 583–588, 2011.

[14] G. Qiao, T. Liu, J. Dai, Y. Hong, and J. Wan, “Qualitative and Quantitative Sensors Based on Electrochemical Techniques for the Corrosion Assessment of RC Panels,” *IEEE Sensors Journal*, vol. 12, no. 6, pp. 2062–2063, 2012.

[15] G. Qiao, Y. Hong, G. Sun, and O. Yang, “Corrosion energy: A novel source to power the wireless sensor,” *IEEE Sensors Journal*, vol. 13, no. 4, pp. 1141–1142, 2013.

[16] W. F. Smith and J. Hashemi, *Foundations of Materials Science and Engineering*, 4th ed. McGraw-Hill, 2005.

[17] J. Raven, K. Caldeira, H. Elderfield, O. Hoegh-Guldberg, P. Liss, U. Riebesell, J. Shepherd, C. Turley, and A. Watson, “Ocean acidification due to increasing atmospheric carbon dioxide,” 2005.

[18] V. Feliu, J. A. González, C. Andrade, and S. Feliu, “Equivalent circuit for modelling the steel-concrete interface. I. Experimental Evidence and theoretical predictions,” *Corrosion Science*, vol. 40, no. 6, pp. 975–993, 1998.

[19] V. Feliu, J. A. González, C. Adrade, and S. Feliu, “Equivalent circuit for modelling the steel-concrete interface. II. Complications in applying the stern-geary equation to corrosion rate determinations,” *Corrosion science*, vol. 40, no. 6, pp. 995–1006, 1998.

[20] S. A. Ouellette and M. D. Todd, “Ultra low-power corrosion-enabled sensor node,” pp. 834523–834523, Apr. 2012.

[21] M. Mellas, B. Mezghiche, and J. E. Ash, “Estimation of the porosity of Portland cement pastes using backscattered electron image,” in *Role of Cement Science in Sustainable Development*, 2003.

[22] S. A. Ouellette and M. D. Todd, “Uncertainty quantification of a corrosion-enabled energy harvester for low-power sensing applications,” p. 86921G–86921G, Apr. 2013.

Scott A. Ouellette received his B.S and M.S. degrees in structural engineering from the University of California – San Diego (UCSD), San Diego, CA, in 2009 and 2011, respectively.

In past summers, he has performed research in the areas of energy harvesting and structural health monitoring at the Engineering Institute of Los Alamos National Laboratory (LANL), Los Alamos, NM. He is currently a National Science Foundation Graduate Research Fellow (NSF-GRF) with UCSD, and is performing research on novel energy harvesting systems.

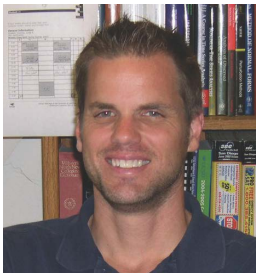

Michael D. Todd received his B.S.E (1992), M.S. (1993), and Ph.D. (1996) degrees from Duke University’s Mechanical Engineering and Materials Science, where he was an NSF Graduate Research Fellow.

From 1996 to 2003, he was with the Fiber Optic Smart Structures Section, U.S. Naval Research Laboratory, Washington, DC, where he was Section Head. In 2003, he joined the Structural Engineering Department at the University of California – San Diego, where he currently serves as Professor and Vice Chair. To date, he has published over 280 journal articles and proceedings, 5 book chapters, and has 4 patents. He conducts research in structural health monitoring strategies, fiber-optic sensor systems, and nonlinear dynamics. He is Campus Director of the UCSD/Los Alamos National Laboratory Engineering Institute.